Muon-spin-rotation and relaxation studies in $(TMTSF)_2$-X compounds

L. P. Le, A. Keren, G. M. Luke, B. J. Sternlieb,* W. D. Wu, and Y. J. Uemura
Department of Physics, Columbia University, New York, New York 10027

J. H. Brewer and T. M. Riseman
Department of Physics, University of British Columbia, Vancouver, Canada V6T 2A3

R. V. Upasani, L. Y. Chiang, W. Kang, and P. M. Chaikin
Department of Physics, Princeton University, Princeton, New Jersey 08544
and Exxon Research and Engineering Company, Annandale, New Jersey 08801

T. Csiba and G. Grüner
Department of Physics and Solid State Science Center, University of California, Los Angeles, California 90024
(Received 1 March 1993; revised manuscript received 30 April 1993)

Muon-spin-rotation and relaxation (μSR) studies of the organic compounds $(TMTSF)_2$-X (X = PF_6, NO_3, and ClO_4) at ambient pressure are reported. We observe spin-density-wave (SDW) states in all three compounds under zero external magnetic field. The onset of the SDW is extremely sharp, which may indicate a first-order transition. The sublattice magnetization (or SDW amplitude) in the PF_6 compound exhibits significant reduction with increasing temperature at low temperatures, which demonstrates the existence of collective low-energy excitations, in addition to the single-particle excitations across the SDW gap. The large spin-wave stiffness we observe in this system is incompatible with a Heisenberg model for a localized spin system; this demonstrates the importance of using an itinerant-electron picture to describe the magnetic behavior of this system. The broad distribution of local magnetic fields deduced from the μSR time spectra is consistent with that expected from an incommensurate SDW. The magnitude of the internal field at $T \rightarrow 0$ is approximately the same for the three systems, suggesting a common SDW amplitude in these systems. Transverse-field μSR measurements in the relaxed-state ClO_4 system show no visible enhancement of the relaxation rate in the superconducting state down to 0.1 K, providing a lower limit for the superconducting penetration depth $\lambda_{ab'} \geq 12\,000$ Å.

I. INTRODUCTION

Conducting organic compounds of the tetramethyltetraselenafulvalene $(TMTSF)_2$-X family, where X denotes a monovalent anion, have displayed many fascinating properties, such as spin-density-wave (SDW) magnetism, superconductivity, anion ordering (AO), field-induced spin-density-wave (FISDW) states, and quantum-Hall-effect (QHE) transitions at low temperatures.[1,2] The interplay and competition between different ground-state instabilities are related to the highly anisotropic electronic structures of these compounds.

In salts with a centrosymmetric anion, such as X = PF_6, an antiferromagnetic SDW ground state is observed at ambient pressure. This state is easily suppressed by applied pressure, resulting in the establishment of superconductivity.[3] On the other hand, salts with a noncentrosymmetric anion, such as $X = NO_3$ and ClO_4, undergo an AO transition. The ground state of the system depends on the degree of anion order and/or disorder produced by cooling conditions of the system near T_{AO}.[4] In the ClO_4 salt, a magnetic SDW phase is stabilized below 4 K in the quenched state produced by rapid cooling,[5] whereas superconductivity appears at 1.2 K in the relaxed state produced by slow cooling.[6] In the case of the NO_3 salt, a SDW phase is obtained with a maximum transition temperature of 12 K following slow cooling. This transition is suppressed under pressure, but no superconductivity is observed up to 24 kbar and down to 50 mK.[7]

Various techniques have been applied in studying the SDW properties.[8–10] However, detailed features, such as the elementary excitations, sublattice magnetization, SDW wave vector, and the order of the phase transition, are open to further investigations. For example, NMR experiments[10] detected the SDW states via the broadening of the resonance line in high applied field. In contrast, muon-spin-rotation (μSR) technique allows a direct observation of the field distribution in zero applied field. This complementary feature is useful for the detailed study of the SDW states. Neutron diffraction is another powerful technique of measuring magnetic order in zero external field, but has not been successful in detecting the SDW ordering in $(TMTSF)_2$-X, presumably due to the small crystal size and small SDW amplitude in the system. We also note that it is difficult to search for a small Bragg peak at an incommensurate wave vector.

Our preliminary zero-field μSR studies[11] on the PF_6 system have demonstrated that μSR is effective for studying magnetic order in organic compounds. Since then, we have extended this study to other compounds of the $(TMTSF)_2$-X family and applied transverse-field μSR to investigate superconductivity in the ClO_4 compound. In this paper, we report the comprehensive results of our studies of $(TMTSF)_2$-X with $X = PF_6$, NO_3, and ClO_4.

II. EXPERIMENTAL ASPECTS

In a μSR experiment,[12] a beam of polarized positive muons is stopped in a target specimen, where the muon spins precess in the local field at frequency $\nu_\mu = (\gamma_\mu/2\pi)B$ (muon gyromagnetic ratio $\gamma_\mu/2\pi = 13.553$ kHz/G). Because of the parity violation of the weak interaction, the decay positron ($\tau_\mu = 2.2$ μs) is emitted preferentially along the muon-spin direction. The time histograms of the accumulated positrons in opposing counters, $N^{\pm}(t)$, reflect the muon local field(s):

$$N^{\pm}(t) = N_0^{\pm} \exp(-t/\tau_\mu)[1 \pm AP(t)] , \tag{1}$$

$$P_s(t) = \int d^3B f(\mathbf{B})[\cos^2\theta + \sin^2\theta \cos(\gamma_\mu B t)] ,$$

where A is the initial asymmetry (typically ~ 0.2) and $P(t)$ is the muon-spin polarization function [the subscript s in Eq. (1) indicates the static-field limit]. $f(\mathbf{B})$ is a function of the local-field distribution, and θ is the angle between the local field and initial muon-spin direction $\mathbf{S}_\mu(0)$. If we neglect the field dependence of θ, the local-field distribution can be derived from the Fourier transform (real part) of the $\sin^2\theta$ term.

In an ordered magnetic system, the $\cos^2\theta$ term in Eq. (1) gives an offset asymmetry and the $\sin^2\theta$ term exhibits an oscillation. In the absence of an external field, the oscillating frequency is proportional to the magnetic order parameter M. Zero-field (ZF) μSR provides an accurate method for monitoring the magnetic properties, especially the temperature dependence of M. By applying a longitudinal field (LF) $\mathbf{H}_L$ parallel to $\mathbf{S}_\mu(0)$, the $\sin^2\theta$ term will be strongly decoupled when H_L is much larger than the static internal field. In contrast, H_L has no effect on the dynamic fields as long as the dynamical fluctuation rate is larger than the Zeeman-level frequency $\omega_L = \gamma_\mu H_L$. Therefore, LF μSR provides a way to separate the effects of dynamic and static fields.

In a transverse-field (TF) μSR, the muon spins precess in an external magnetic field $\mathbf{H}_{\rm ext}$ normal to $\mathbf{S}_\mu(0)$. The inhomogeneity of the local magnetic field can be determined from the depolarization rate σ of the oscillation. In a type-II superconductor,[13] when $H_{c1} \ll H_{\rm ext} \ll H_{c2}$, the field width ΔB due to the flux-lattice structure is nearly independent of $H_{\rm ext}$: $\sigma \propto \Delta B \propto \lambda^{-2}$. Thus, the superconducting penetration depth λ can be deduced from the results of a TF-μSR measurement in the mixed state of a superconducting specimen. Figure 1 shows a schematic view of the experimental configurations for these three different types of μSR measurements.

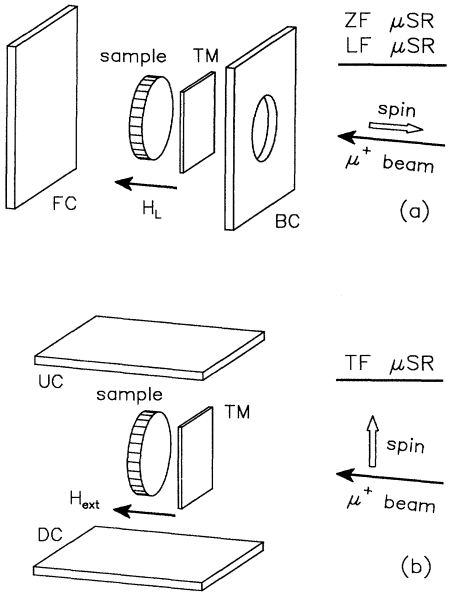

FIG. 1. Schematic view of the μSR experiment configuration. The polarized muon beam is identified by TM, and the decay positrons are detected by opposing counters FC/BC and UC/DC. The external fields (H_L and $H_{\rm ext}$) are applied along the beam direction for the LF and TF-μSR studies.

Single crystals of $(TMTSF)_2$-X were prepared by the usual electrochemical method. The typical dimensions of a crystal were $7 \times 0.5 \times 0.3$ mm^3, with the highest electronic conducting a axis along the needle direction and the least conducting c^* axis along the shortest dimension. A mosaic of specimens (totally about 200 mg) was mounted in a helium-4 gas flow cryostat [and also in an Oxford Instruments model 400 top-loading dilution refrigerator (DR) for the PF_6 compound] for investigation of the SDW ordering. In the case of the ClO_4 salt, the effects of superconductivity were examined in a DR. The PF_6 crystals were randomly arranged but with their a axes normal to the beam direction. The NO_3 and ClO_4 crystals, on the other hand, were oriented with their a axes horizontal and the largest ab' plane normal to the beam direction. The experiments were all performed at the M15 and M20 surface muon channels at TRIUMF.

III. RESULTS IN $(TMTSF)_2PF_6$

The PF_6 single crystal was studied by ZF μSR from 25 K down to 0.1 K with $\mathbf{S}_\mu(0)$ parallel to the muon-beam direction. Figure 2(a) shows the μSR time spectra at several temperatures. The system undergoes a magnetic transition at $T_{\rm SDW} = 12.2$ K. Above $T_{\rm SDW}$, the time spectra are essentially the same: The muon spins are depolarized slowly by a small local field of about 3 G. We attribute this small field to (randomly oriented) static nuclear dipolar fields. Below $T_{\rm SDW}$, the muon-spin depolarization is enhanced and is accompanied by the ap-

pearance of oscillations. This clearly indicates the onset of SDW magnetic order below 12.2 K, in agreement with previous studies.

Figure 2(b) shows the Fourier transform of a time spectrum taken at 3.7 K. We have removed the slowly decaying offset asymmetry in time space to subtract a sharp peak near zero frequency. The frequency distribution in Fig. 2(b) roughly reflects the local-field distribution. The peak near 0.55 MHz corresponds to the oscillating signal, while the remaining spectral weight below 0.55 MHz reflects the quickly relaxing signal seen in Fig. 2(a). The broad nature of the frequency distribution may be attributed to either an incommensurate SDW or multiple muon locations. We provide detailed discussions in Sec. VI concerning the comparison of these two cases with experimental results.

The ZF spectra below T_{SDW} were fit with a phenomenological form:

$$AP(t) = A_1 \exp(-\sigma_1^2 t^2/2)\cos(2\pi\nu_\mu t + \phi) + A_2 \exp(-\sigma_2 t) + A_3 \exp(-\sigma_3 t)\,, \qquad (2)$$

where A_n is the asymmetry and σ_n is the Gaussian or exponential relaxation rate of each signal. The combination of the first and second terms approximately represents the frequency distribution shown in Fig. 2(b), while the third term corresponds to the offset asymmetry due to the $\cos^2\theta$ term of Eq. (1) and the signal due to the small local field. The weak time dependence of the last term could be ascribed to the relaxation of either a small static field or dynamic effects. These effects in the PF_6 salt will be clarified in Sec. VI. Values for the total asymmetry and ϕ were held constant for all the fits.

Figure 3 shows the temperature dependence of A_n and σ_n. (Data for A_n and σ_3 measured in the dilution refrigerator are not shown, since their values are sensitive to the different experiment configuration.) While A_n and σ_3 show little temperature dependence, σ_1 and σ_2 exhibit a slow decrease with increasing temperature followed by a reduction near T_{SDW}. Possible trade-off effects among the three signals are checked in the following way. Since $\sigma_2 \gg \sigma_3$, it rules out exchange between the second and third terms. The absence of any enhancement of σ_3 just below T_{SDW} ensures the separation between the first and

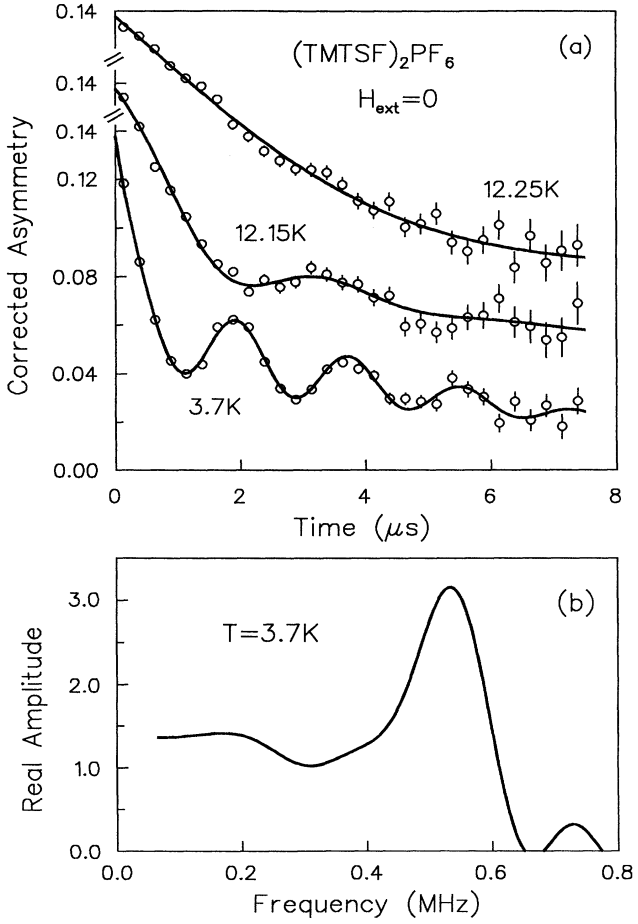

FIG. 2. Zero-field muon-spin-rotation results in $(TMTSF)_2PF_6$. (a) μSR time spectra at $T = 3.7$ K, 12.15 K, and 12.25 K. The clear onset of depolarization due to static magnetic order is seen below $T_{\mathrm{SDW}} = 12.2$ K. There is no change of the spectral weight below 10 K. (b) Fourier transform of time spectrum at 3.7 K. The real part of the Fourier transform reflects the local-field distribution.

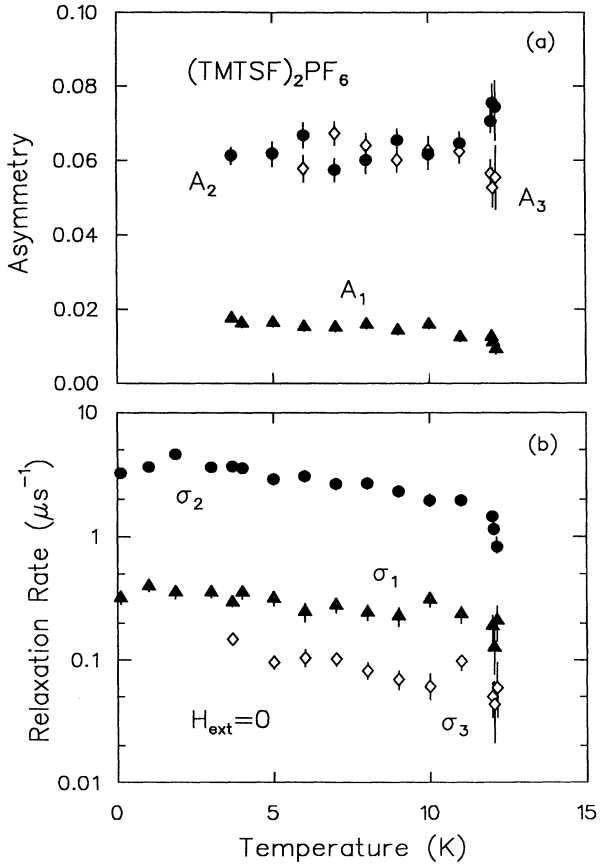

FIG. 3. Temperature dependence of ZF-μSR asymmetry A_n and relaxation rates σ_n in $(TMTSF)_2PF_6$. A_n and σ_n are defined according to Eq. (2).

third terms. The temperature variation of σ_2 and σ_1 [Fig. 3(b)] is similar to that of ν_μ (Fig. 4). This indicates that the shape of the field distribution is nearly independent of T in the whole temperature range below T_{SDW}.

IV. SDW ORDER PARAMETER IN $(TMTSF)_2PF_6$

The temperature dependence of the SDW amplitude M can be studied by deriving the frequency of the oscillation seen in the time spectra. The peak frequency, which corresponds to the muon local field with the largest spectral weight, is proportional to M, *independent* of the assumption of whether the SDW in the PF_6 system is commensurate or incommensurate.

Figure 4 shows the temperature dependence of ν_μ (solid circle). As a comparison, we also show the peak-to-peak width of the absorption derivative $\Delta H_{p.p.}$ obtained by proton NMR (Takahashi *et al.*,[14] open circle) with $H_{ext} = 11.7$ kG. Below T_{SDW} the temperature dependence of ν_μ and $\Delta H_{p.p.}$ agrees fairly well. However, the present results provide much better statistical accuracy and demonstrate the sharp transition at T_{SDW} and the slow variation of ν_μ at low temperatures more clearly than NMR.

In ZF μSR, the system lies in the SDW ground state and $\nu_\mu \propto M$. In NMR measurements, the external field of 11.7 kG applied in the $b'c^*$ plane leads to the establishment of a spin-flop state in the system, where $\Delta H_{p.p.}$ is also proportional to M. The agreement between these two experiments suggests that the PF_6 salt exhibits similar $M(T)$ in both the ground and spin-flop states. The dashed line in Fig. 4 shows the BCS gap in the weak-coupling limit; a mean-field theory[15] predicted the same temperature dependence of $M(T)$. The present μSR data, however, are significantly different from the BCS form or the sublattice magnetization curves of usual antiferromagnets.

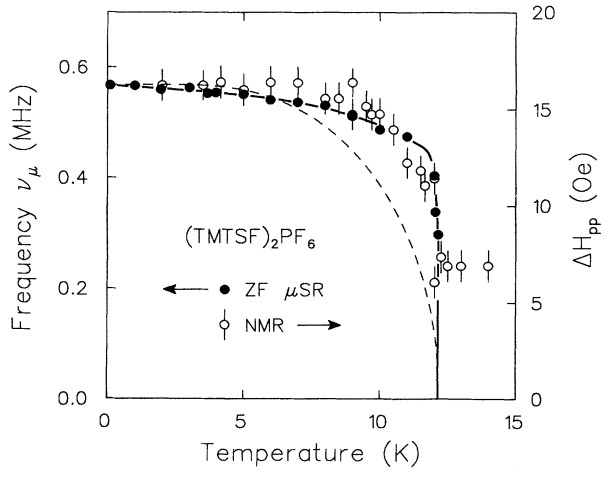

FIG. 4. Zero-field muon-spin precession frequency ν_μ observed in $(TMTSF)_2PF_6$. As a comparison, the proton-NMR results of the peak-to-peak width of absorption derivative, $\Delta H_{p.p.}(T)$, are also included. The solid line is a guide to the eye, and the dashed line corresponds to the energy gap in the BCS weak-coupling theory. The sharp change near the transition temperature in the μSR data suggests a possibility of a first-order transition.

The sharp transition in the PF_6 salt may be ascribed to the low dimensionality of the system. In general, long-range order does not exist in purely one-dimensional (1D) systems at any finite temperature because of strong fluctuations of the order parameter.[16,17] Because of this effect, the Peierls transitions in quasi-1D systems occurs at temperatures T_{SDW} lower than those given by mean-field calculations.[18] Accordingly, the SDW fluctuations have already developed at temperatures above T_{SDW}. As the temperature decreases, the system crosses over from 1D to 3D and long-range static magnetic order appears.[17] Since the fluctuating order parameter exists above the transition temperature, the static magnetic order parameter frozen at T_{SDW} may have a finite value (first-order transition). Alternatively, this mechanism would enhance the sharp increase of the order parameter below the transition temperature even for the case of a second-order transition. Recent transport experiments on unstrained crystals,[19] and more recent proton-NMR measurements on a single crystal,[20] have been interpreted as demonstrating a sharper, first-order-like transition. A sharp first-order transition followed by a small change of the low-temperature sublattice magnetization was also observed in antiferromagnetic Cr, which exhibits SDW ground state.[21]

The temperature dependence of the magnetization we observed is distinctly different from the temperature dependence of the order parameter obtained within the mean-field treatment of the SDW transition.[15] This treatment leads to $\Delta(T)$, which is identical to the BCS expression for the superconducting gap. The single-particle gap has been established by temperature-dependent transport studies,[22] and such experiments also lead to a gap value close to that in the weak-coupling limit. The gap, and consequently the magnetization, if determined by single-particle excitations, is essentially temperature independent below about $T_{SDW}/2$. Therefore, the unsaturated temperature dependence of the magnetization observed at low temperatures (solid circles in Fig. 5) must be of different origin.

We argue that the variation of $M(T)$ at low temperatures is determined by collective spin waves rather than by single-particle excitations. The static magnetic properties of a SDW ground state have been analyzed in terms of a Heisenberg antiferromagnet with anisotropic exchange constants $J_\parallel$ and $J_\perp$. Such a description also accounts for the observed antiferromagnetic resonance frequencies.[9] These experiments lead to the on-chain exchange coupling $J_\parallel$, but no information is gained on the exchange coupling perpendicular to the chains $J_\perp$. Because of the strongly anisotropic band structure, which has two widely different bandwidths in the two directions perpendicular to the chains, we assume that $J_\perp$ along the c^* axis is negligible. The low-lying excitations are thus described by a two-dimensional, $S = 1/2$ Heisenberg model. The Hamiltonian is given by

$$\mathcal{H} = \alpha^2 \sum_{i,\delta} J_\delta \mathbf{S}_i \cdot \mathbf{S}_{i+\delta} , \quad (3)$$

with $\alpha = \mu/\mu_B$ representing the magnitude of the SDW modulation.[23] We shall not need to restrict J_δ to be the nearest-neighbor (NN) interaction, and generally it is a function of the (2D) distance δ.

Since the reduction of M in the temperature range of interest is rather small, for instance, $\Delta M/M \approx 6\%$ at 8 K, we write the dispersion relation of magnon modes in a long-wave approximation:

$$\omega_k^2 = D^2(ka)_{\|}^2 + D'^2(ka)_{\perp}^2 + \Delta^2 , \quad (4)$$

where D (D') is the intrachain (interchain) stiffness constant and Δ is the anisotropy gap. The magnitude of D (D') depends on the details of the exchange coupling J_δ. In the $(TMTSF)_2$-X salts antiferromagnetic resonance experiments[9] lead to two anisotropy gaps (see below). Consequently, the density of states and the cutoff frequency are given by (we use $\hbar = 1$ and $k_B = 1$)

$$\rho(\omega) \approx 2\omega/\omega_{\rm cut}^2 ,$$
$$\omega_{\rm cut}^2 \approx 2\pi DD' .$$

The reduction of the magnetization at temperature T is given by

$$\frac{\Delta M}{M} \approx \sum_{n=1}^{2} \int_{\Delta_n}^{\omega_{\rm cut}} \frac{\alpha J}{\omega_n} \frac{\rho(\omega_n) d\omega_n}{\exp(\omega_n/T) - 1}$$
$$\approx \sum_{n=1}^{2} \frac{2\alpha JT}{\omega_{\rm cut}^2} \ln\left[\frac{1 - \exp(-\omega_{\rm cut}/T)}{1 - \exp(-\Delta_n/T)}\right] ,$$

$$J = \sum_{\delta}^{d} J_\delta ,$$

where the effective exchange interaction J is the summation of all exchanges on the different sublattices.[24] In the temperature range of interest, $\Delta \ll T \ll \omega_{\rm cut}$, we have

$$\frac{\Delta M}{M} \approx \frac{2\alpha JT}{\pi \overline{D}^2} \ln\left(\frac{T}{\overline{\Delta}}\right) , \quad (5)$$

with the average $\overline{D}$ and $\overline{\Delta}$ defined as $\overline{D}^2 = DD'$ and $\overline{\Delta}^2 = \Delta_1\Delta_2$, respectively.

The parameter J is related to the magnitude of the perpendicular spin susceptibility $\chi_\perp$, and $J = 1200$ K is deduced from $\chi_\perp$ in the PF_6 salt.[25] The anisotropy gap is rather small; for instance, in the AsF_6 salt antiferromagnetic resonance (AFMR) measurements[9] determined that $\Delta_1 = 0.1$ K and $\Delta_2 = 0.3$ K, respectively. α is estimated to be about 0.1 by proton-NMR experiments.[10] Using $J = 1200$ K, $\overline{\Delta} \approx 0.2$ K, $\alpha \approx 0.1$, and $\Delta M/M \approx 6\%$ at 8 K, we obtain the average stiffness constant $\overline{D} \approx 200$ K. The calculated magnetization $M(T)/M(0)$ with $\overline{D} \approx 200$ K is shown in Fig. 5 (solid line). We also show the temperature dependence of the single-particle gap as obtained from weak-coupling BCS theory (dashed line).

Based on Fig. 5 we conclude that at low temperatures $M(T)$ is determined by collective excitations, with single-particle excitations playing only a minor role. This analysis raises several interesting questions concerning the nature of the phase transition in these TMTSF salts. Our analysis applies only at low temperatures where magnon-magnon interactions and the temperature-dependent reduction of the single-particle gap can be neglected. At higher temperatures these effects are important, but which of these two mechanisms is primarily responsible for the phase transition remains to be seen. It should also be interesting to see if the observed stiffness constant $\overline{D} \approx 200$ K is consistent with localized-moment magnetism or with an itinerant-electron picture. We discuss these points in Sec. VIII.

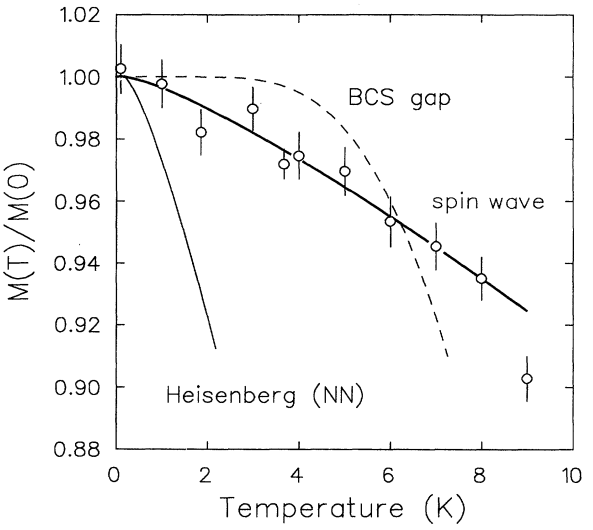

FIG. 5. Comparison of μSR data at low temperatures with model calculations. The thick solid line shows the 2D spin-wave calculation with an average stiffness constant of 200 K, the dashed line represents the weak-coupling BCS-gap curve, and the thin solid line shows the result for the Heisenberg model with only nearest-neighbor interactions.

V. SDW ORDERING IN $(TMTSF)_2$-X

Similar experiments were carried out in the NO_3 system, with $\mathbf{S}_\mu(0) \parallel$ the b' axes of the specimens. The samples were precooled though $T_{\rm AO} = 41$ K with a cooling rate of 0.15 K/min in zero external field. SDW order appears below 9.1 K, and the μSR time spectra are essentially similar to those observed in the PF_6 salt. Figure 6 shows the time spectrum at 3.2 K. The fast relaxing signal visible in the first microsecond reflects the wide field distribution. The spectra were analyzed according to Eq. (2), and the results of $\nu_\mu(T)$ are shown in Fig. 7. We see a slow variation of ν_μ at low temperatures followed by and a sharp change of ν_μ near $T_{\rm SDW}$, features which are similar to those observed in the PF_6 salt. The $T_{\rm SDW} = 9.1$ K obtained in our experiment is lower than the 12 K obtained by transport measurements.[26] This may be due to the cooling rate around $T_{\rm AO}$.

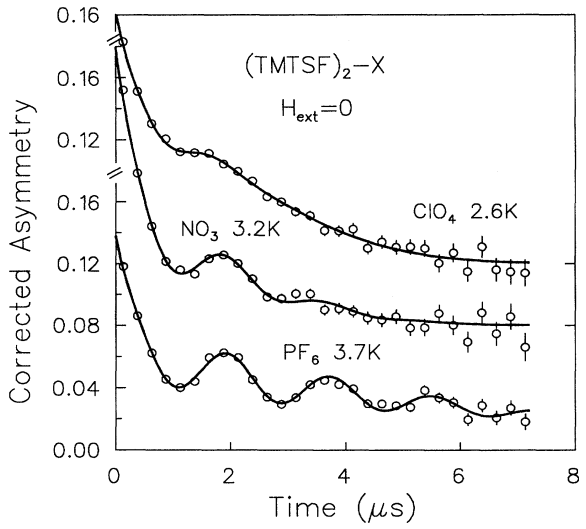

FIG. 6. ZF-μSR time spectra observed in (TMTSF)$_2$-X below T_{SDW}. The depolarization and oscillation due to SDW magnetic order are seen in the PF_6, NO_3, and ClO_4 systems.

We have also observed SDW ordering in the ClO_4 system, with $\mathbf{S}_\mu(0) \parallel b'$. The system was first precooled rapidly from 70 K to 5 K in 20 s, resulting in the formation of a quenched state. $T_{SDW} = 4.1$ K at this cooling rate. Figure 6 shows the ZF time spectra at 2.6 K. The oscillating signal and nonoscillating base line ($\cos^2\theta$ term) relax much faster than those in the PF_6 and NO_3 compounds at low temperatures. The temperature dependence of ν_μ in the ClO_4 salt is shown in Fig. 7. Since the oscillating signal is less pronounced, the results for ν_μ are less accurate. However, a rather sharp transition

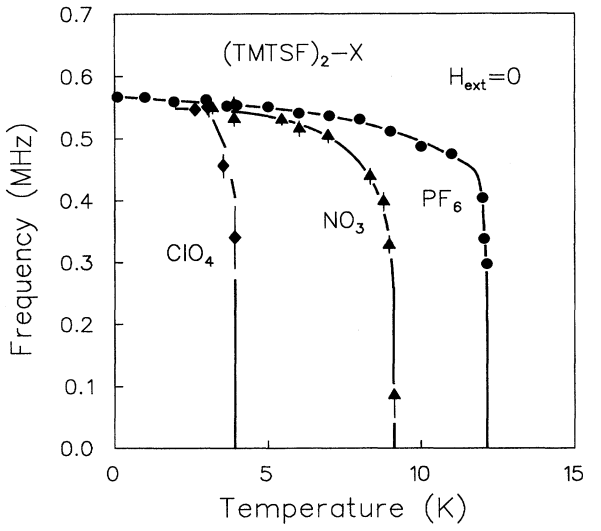

FIG. 7. Temperature dependence of the muon-spin precession frequency in zero field observed in (TMTSF)$_2$-X. The PF_6, NO_3, and ClO_4 compounds show roughly the same precession frequency at zero temperature.

near T_{SDW} is still visible, similar to that observed in the PF_6 and NO_3 salts.

Figure 7 demonstrates that the muon precession frequencies at low temperatures are essentially system independent (the difference is less than 10%), while the transition temperatures are remarkably different (from 12.2 to 4.1 K). We note that ν_μ depends on both M and the muon location. If we assume that the muon sites are essentially same in the TMTSF family, our results then indicate that $M(T \to 0)$ is similar for these compounds. At the moment, we cannot rule out the possibility of different muon sites. Such a situation is, however, less likely since in this case one must assume that the effects of the muon site and M are accidentally and perfectly canceled out. A similar result has been obtained by NMR measurement of the pressure dependence of M in the PF_6 salt.[27] The NMR experiment shows that while T_{SDW} was strongly suppressed under pressure, $M(T \to 0)$ was found to have no pressure dependence.

It was suggested[27] that this feature was a direct support of the nesting model for SDW condensation. In the (TMTSF)$_2$-X family, the interchain coupling t' is anion (or, alternatively, pressure) sensitive, whereas the on-site Coulomb energy U and the on-chain coupling t remain almost constant. Following the nesting model,[15] the order parameters, such as Δ_{SDW} and M, are mainly determined by the mechanism of the electron-electron interaction, namely, the on-site Coulomb energy and t, whereas the transition temperature itself is very sensitive to t'. A BCS-like relation of $\Delta_{SDW} \propto T_{SDW}$ holds only for the maximum transition temperature or perfect nesting (such as in the PF_6 salt). With increasing dimensionality (2D character) of the system, the nesting of the Fermi surface becomes less perfect. An energy ϵ_0, corresponding to the violation of perfect nesting, increases with increasing t'. The competition between Δ_{SDW} and ϵ_0 leads to a reduction of T_{SDW} (such as in the ClO_4 salt) though M stays rather constant. When ϵ_0 exceeds Δ_{SDW}, the SDW phase disappears abruptly.

Table I shows the 2D anisotropy of conductivity $\sigma_a/\sigma_{b'}$ versus the SDW transition temperature in (TMTSF)$_2$-X. The 2D anisotropy can be reduced by either increasing the pressure in the PF_6 compound or replacing the PF_6 by ClO_4 salt at ambient pressure. With decreasing anisotropy, T_{SDW} drops monotonically. The present

TABLE I. Anisotropy vs T_{SDW} in (TMTSF)$_2$-X.

Compound	P (kbar)	$\sigma_a/\sigma_{b'}$ at 300 K	T_{SDW} (K)
PF_6	0	200[a]	12.2
PF_6	3		10.5[b]
PF_6	6.5		6.5[b]
PF_6	10	7[c]	0
PF_6	0	200[a]	12.2
NO_3	0	$\sim$ 200[a]	9.1
ClO_4	0	23[d]	4.1

[a]See Ref. 28.
[b]See Ref. 27.
[c]See Ref. 29.
[d]See Ref. 30.

experiments in the TMTSF system with various anions and previous NMR experiments in the PF_6 salt under different pressures also show that M is insensitive to the anisotropy as long as the SDW ground state exists. These results confirm two basic predictions of the Fermi-surface nesting model for the SDW in TMTSF compounds.

VI. SDW PROPERTIES AND MUON LOCAL FIELDS

In a μSR experiment, the muon is localized at a site with a minimum electrostatic potential shortly after implanted into the specimen. The muon spin precesses in the local field of the muon site. In the following, we present a model calculation for the local-field distribution expected for an incommensurate SDW (ICSDW) and a commensurate SDW (CSDW), and compare the results with the observed data.

Figure 8(a) shows the shape of the local-field distributions $f(B)$ for both the commensurate and incommensurate modulations. Here, we assume that the muon local field $B(x)$ is directly proportional to the local spin density $S(x)$, which varies with the sinusoidal modulation. Contributions from nuclear dipolar fields are not included. For CSDW, $f(B)$ is a δ function, because the crystallographically symmetric muon sites always "see" the same phase of SDW modulation. For an ICSDW, $f(B)$ represents a sinusoidal distribution

$$f_s(B) = \begin{cases} (2/\pi)(B_{\max}^2 - B^2)^{-1/2} & \text{if } B < B_{\max}, \\ 0 & \text{otherwise}. \end{cases} \quad (6)$$

We see that $f_s(B)$ has finite values below the maximum field $B_{\max}$ and diverges at $B_{\max}$. Figure 8(a) demonstrates a broad field distribution in the ICSDW. In contrast, the field distribution is very sharp for the CSDW.

If the local field is due predominantly to the contact hyperfine interaction, $B(x) \propto S(x)$ and the corresponding $f(B)$ is shown in Fig. 8(a). Alternatively, we can study $f(B)$ assuming that the local fields result predominantly from the atomic dipolar fields of the spin density, similar to our analysis in the cuprate systems.[31] Here, we assume that the intermolecular spin-density amplitude is sinusoidally modulated with a wave vector of $\mathbf{Q} = (0.5, 0.24, -0.06)$,[10] the spin-density distribution within a molecule is determined by electron-spin resonance (ESR),[32] and the spin orientation $\mathbf{s}$ is taken to be along the b' axis as found in the AsF_6 salt:[8]

$$\mathbf{B} = M \sum_{i,j} \frac{-\mathbf{s} + 3(\mathbf{s} \cdot \mathbf{n}_{ij})\mathbf{n}_{ij}}{|\mathbf{R}_i + \mathbf{r}_j - \mathbf{R}_\mu|^3} \rho_j \cos(\mathbf{R}_i \cdot \mathbf{Q}) , \quad (7)$$

where $M \approx 0.1\ \mu_B$/molecule,[10] $\mathbf{n}_{ij}$ is the unit vector from the muon to a spin density ρ_j at jth atom $\mathbf{r}_j$ in ith molecule $\mathbf{R}_i$, and $\mathbf{R}_\mu$ is the considered muon site.

The observed maximum local field of 40 G, derived from the peak frequency 0.55 MHz, is an order of magnitude smaller than those in the insulating parent compounds of cuprates.[31] This result may be interpreted in terms of both the small value of M and the large molecule size in the TMTSF compounds. Generally, knowledge of the muon site is important to determine the magnitude of the local field. The muon location is, however, less significant in determining the field distribution, especially in an incommensurate magnetic system, where the broad field distribution is due mainly to the intermolecular spin-density distribution. We consider a particular muon site at $(0.17, 0.75, 0.24)$, where the maximum local field is 40 G.

Figure 8(b) compares the calculated $f(B)$ for both the incommensurate wave vector $\mathbf{Q}$ (solid line) and the commensurate wave vector $\mathbf{Q}_0 = (1/2, 1/4, 0)$ (dashed line). In both cases, we have also included a small inhomogeneity of the local field due to the nuclear dipolar fields of 3 G, which corresponds to the relaxation rate observed above T_{SDW}. Because of the quick decay of the dipolar field as r^{-3}, the magnetic-field contribution from the spin density outside the local molecule is negligibly small. As a result, the shape of the field distribution is rather insensitive to a variation of the wave number $\mathbf{Q}$, as long as

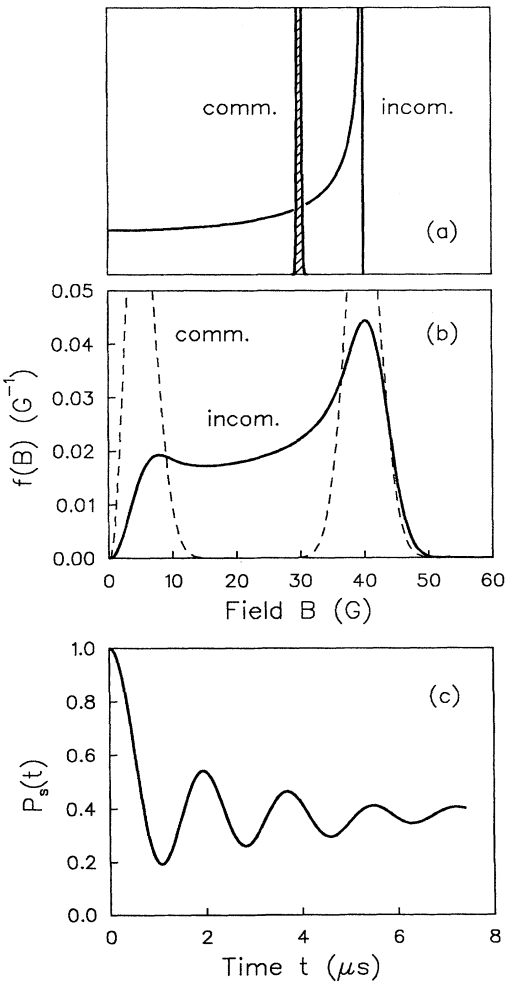

FIG. 8. Model calculation of SDW. (a) Local-field distribution for commensurate and incommensurate SDW's, assuming $B(x) \propto S(x)$. (b) Local-field distribution derived from Eq. (5) after adding nuclear dipolar broadening. (c) μSR time spectra based on the above incommensurate field distribution and present experiment configuration.

it is incommensurate. The peak near the largest possible field is due to the sharp peak of $f_s(B)$ shown in Fig. 8(a). Since the fields from various sources point in different directions, the summation of these fields generally will not be canceled out. A small peak near 5 G, corresponding to a muon site where the local spin density is extremely small, reflects the magnitude of the dipolar contribution from the spin density in the neighbor molecules. Based on this model the μSR time spectra can be evaluated according to Eq. (1). The results of $P_s(t)$ for the ICSDW are shown in Fig. 8(c). The simple model calculation agrees fairly well with the observed results (Fig. 2): The oscillating and fast relaxing behaviors are clearly seen.

Because of the nuclear dipolar field, the δ function for the CSDW acquires a width of about 3 G. Since the peak for the original sinusoidal distribution in the ICSDW is rather sharp, the linewidth at the peak field for the ICSDW is only sightly ($\sim$ 50%) larger than that for the CSDW [Fig. 8(b)]. The observed results of $\sigma_1 = 0.3$–0.4 μs^{-1} at low temperatures, corresponding to a linewidth 4–5 G, are about 50% larger than the nuclear dipolar broadening of 3 G. Therefore, the width of the peak field can be explained by the incommensurate model.

The present μSR measurements are consistent with the ICSDW in the PF_6 salt. However, the μSR data alone cannot definitely rule out the possibility of a CSDW, since we do not know the muon location(s) in the unit cell. In order to explain the observed results with a commensurate model, one has to assume more than four different muon sites within the unit cell, with particular occupancy probability, to account for the broad distribution observed at lower fields. This scenario is less attractive than the simpler model of a unique site with an incommensurate modulation. Our recent μSR measurements[33] in the organic ferromagnet of β-phase p-NPNN showed a long-lived oscillation with a unique frequency, indicating a well-defined muon local field in a commensurate spin structure. This demonstrates that a single muon site is possible even in a complicated organic system (there are 36 atoms within each NPNN molecule). These arguments suggest that the observed results can be better explained by an ICSDW than a CSDW.

The SDW properties in $(TMTSF)_2$-X have been investigated by NMR experiments. The SDW have been found to be incommensurate in both the PF_6 and ClO_4 salts.[10] A recent NMR measurement in $(TMTSF)_2PF_6$ and $(TMTTF)_2Br$ (Ref. 34) clearly demonstrate different line shapes in the SDW state of these two systems: the ICSDW in the PF_6 salt versus the CSDW in the Br salt (cf. Fig. 2 in Ref. 34). Once we accept an ICSDW in the PF_6 salt, the current study rules out a possible incommensurate-to-commensurate transition down to 0.1 K, since there is no significant change of μSR spectral weight in our measured temperature range.

A slow relaxation of the nonoscillating signal in the time spectra (Fig. 2) may be ascribed to either the effect of dynamic fluctuating fields or the small static local fields. These two effects can be distinguished by applying a longitudinal field large enough to decouple small static fields. Figure 9 shows the result of LF spectra at several fields. With an applied field of only 20 G the slowly relaxing signal is strongly suppressed (flat tail). This clearly indicates that dynamic effects in our system are negligible,[35] which validates our analysis in the static magnetic-field limit. The small static field may be connected to the nuclear dipolar fields within the sample container or a possible nonmagnetic volume within the sample. This signal occupies about 25% of the total spectral weight.

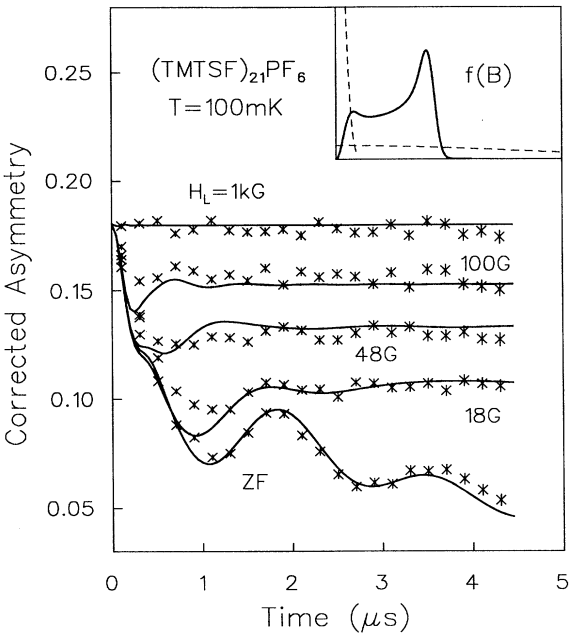

FIG. 9. LF-μSR time spectra observed in $(TMTSF)_2PF_6$ at 0.1 K. The solid lines show the model calculation based on the local-field distribution shown in the inset for the incommensurate SDW.

It is interesting to further compare the incommensurate SDW model with the LF time spectra. The experimental data show a rather weak decoupling effect, indicating more weight for the larger fields. After adding $\approx$ 20% spectral weight of random field with a width of 80 G, the model calculation (the solid lines in Fig. 9) fits the LF-μSR data reasonably well. The field distribution is shown in the inset of Fig. 9, with a solid line for the incommensurate SDW field distribution and dotted line for the random field contribution. The larger local fields may be due to the second muon site which is located closer to a spin carrier. In general, the ZF-μSR spectra are sensitive to the peak in the field distribution but fairly insensitive to the small spectral weight of the high-field tail in the field distribution, which gives a fast relaxing signal in a short time. LF μSR, on the other hand, can detect the field distribution more precisely by changing the applied field. Since the higher-field weight is rather small ($\approx$ 20%), our conclusion of incommensurate SDW formation is essentially unaffected by the observation of the high-field site.

The model calculations in Figs. 8 and 9 agree well with the observed results in the PF_6 system (Fig. 2). However,

the μSR spectra in the NO_3 and ClO_4 systems show much higher relaxation rates (Fig. 6), indicating greater inhomogeneity of the static fields at the muon sites. This phenomenon may be related to the existence of an AO transition in the latter two compounds. Anion disordering introduces a small random electric field to the periodic molecular fields. Since the muon site is sensitive to the electrostatic potential, the effective spatial spread of the muon site could increase with a decreasing degree of the anion ordering. In the relaxed ClO_4 salt, for example, the maximum degree of anion disorder leads to the largest inhomogeneity of the local fields.

Figure 10 shows the quantitative results of the local field and the μSR spectra due to the spatial spread of the muon site. Around a particular muon site of $(0.17, 0.75, 0.14)$, the local field (corresponding to the peak in the field distribution) changes by 50% when a muon deviates from the center location by 0.3 Å [Fig. 10(a)]. The μSR time spectra with various sizes ΔR_μ of the muon site are shown in Fig. 10(b). The relaxation of the nonoscillation asymmetry [$\cos^2\theta$ term in Eq. (1)] is taken into account by assuming $P(t) = P_s(t)\exp(-\nu t)$. With values of $\Delta R_\mu = 0.1$ and 0.2 Å, $\nu = 0.1$ and 0.2 μs^{-1}, the model results [dashed and dot-dashed lines in Fig. 10(b)] display essentially the same feature with the ZF-μSR spectra seen in the NO_3 and ClO_4 compounds (Fig. 6), respectively.

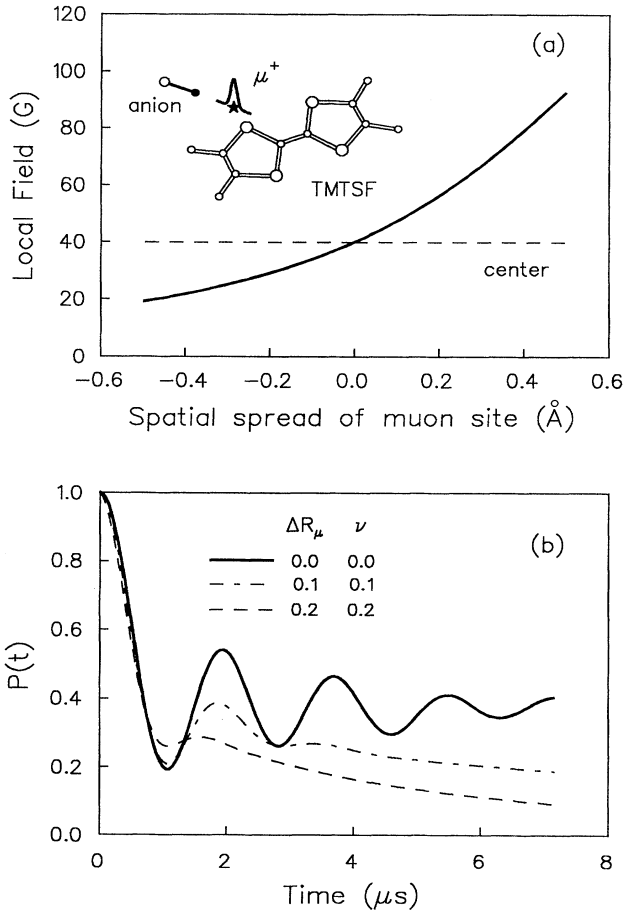

FIG. 10. Model calculation for the effect of finite spatial extent of the muon site. (a) Local field versus deviation of muon site from the equilibrium location, where the local spin density has a maximum value. (b) μSR time spectra vs the effective size of the muon site ΔR_μ and the base-line relaxation ν.

VII. SUPERCONDUCTIVITY IN $(TMTSF)_2ClO_4$

The superconducting phase of the ClO_4 salt was obtained by slowly cooling the crystals at a rate of about 0.05 K/min below 30 K. The sample was field cooled in $H_{ext} = 180$ G applied perpendicular to the most highly conducting ab' plane. Figure 11 shows TF-μSR time spectra in a rotating reference frame. The spectra above and below the superconducting transition temperature ($T_c \approx 0.8$ K) exhibit almost identical behavior. Figure 12 shows the temperature dependence of the muon precession frequency [Fig. 12(a)] and the transverse-field relaxation rate [Fig. 12(b)] obtained from fits of the time spectra. A negative frequency shift below 0.8 K indicates the onset of the superconductivity. The frequency shift corresponding to $\overline{B(T_c)} - \overline{B(0)} \approx 0.1$ G is mainly due to the superconducting diamagnetic shift and Lorentz and demagnetizing shifts below T_c. The relaxation rate $\sigma(T)$, on the other hand, fails to display any visible enhancement below 0.8 K. Such behavior was also reported in previous μSR measurements[36] in the heavy-fermion superconductors UPt_3 and UBe_{13} with an applied field well above H_{c1}. The enhancement of the relaxation rate due to superconductivity is $\sigma_{sc}(T) = \sqrt{\sigma^2(T) - \sigma^2(T_c)} \propto \lambda^{-2}$. A negligibly small $\sigma_{sc}(T \to 0)$ suggests that the magnetic penetration depth in the ClO_4 compound is extremely large. We estimate an upper limit for $\sigma_{sc}(T \to 0)$ of 0.05 μs^{-1}, giving a penetration depth in the conducting

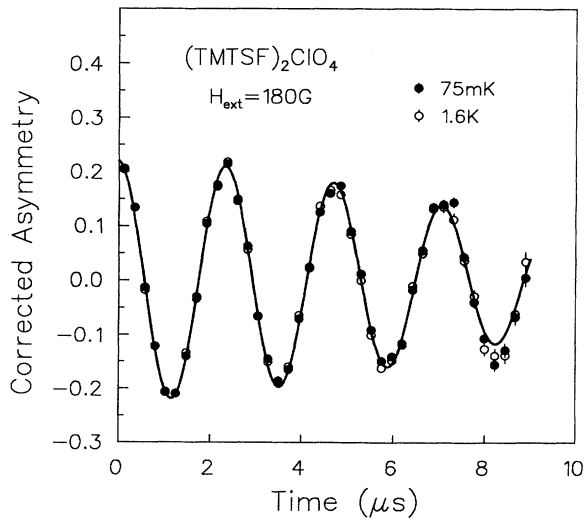

FIG. 11. TF-μSR time spectra in the quenched state of $(TMTSF)_2ClO_4$. The sample was field cooled in $H_{ext} \approx 180$ G applied perpendicular to the ab' plane. No significant change of the μSR spectra is observed around $T_c \approx 0.8$ K.

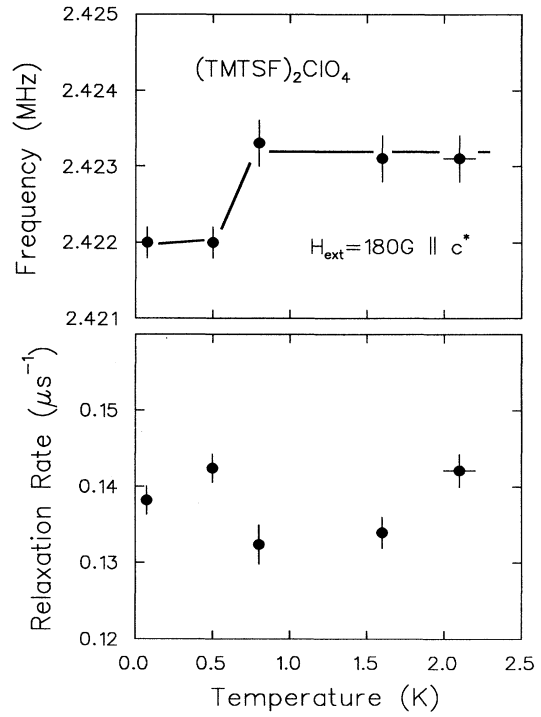

FIG. 12. Field-cooled measurements in $(TMTSF)_2ClO_4$. (a) Muon-spin precession frequency vs temperature. The negative frequency shift below 0.8 K is attributed to the onset of superconductivity. (b) Relaxation rate σ vs temperature. No visible enhancement of σ is seen below 0.8 K.

plane $\lambda_{ab'} \geq 12\,000$ Å.

Previous measurements of the upper critical field in the ClO_4 system[37] show that $H_{c2} = 1.6$ kG as $\mathbf{B}_{\text{ext}} \parallel c^*$ axis, yielding an average in-plane coherence length $\xi = 450$ Å. Combining with the thermodynamic critical field $H_c = 44$ G obtained by specific-heat measurement,[38] we derive the Ginzburg-Landau parameter $\kappa = 26$ and $\lambda = 12\,000$ Å, which is in agreement with the μSR results. With this value of λ, it is possible to further estimate the superconducting carrier density n_s and Fermi temperature T_F. Superconductivity in the ClO_4 salt appears as the result of the suppression of 1D character, and the penetration depth we obtained above is an average value in the 2D ab' plane. Here we discuss using a model for 2D systems, so that we can compare this system with other superconductors. The electronic mean free path ($l = 14\,000$ Å according to Ref. 39) is much longer than the coherence length in the ab' plane, $l \gg \xi$. The system, therefore, lies in the clean limit, where $n_s \propto m^*/\lambda^2$. In a 2D system, the effective mass m^* can be deduced from the electronic specific-heat measurements: the Sommerfeld constant $\gamma \propto m^*$. A value[38] of $\gamma = 10.5$ mJ/mol/K^2 yields $m^* \approx 2.0 m_e$. We estimate $n_s \approx 4 \times 10^{19}$ cm^3, which is about 3% of the carrier density expected assuming one carrier per formula unit. For the Fermi temperature, $T_F \propto n_s/m^*$ in a 2D system; we estimate $T_F \approx 70$ K in the ClO_4 salt. The Fermi temperature T_F, derived from the penetration depth in this way, represents a typical energy scale of superconducting carriers. As discussed in Ref. 40, however, T_F does not necessarily correspond to the difference in the single-particle energies between the bottom and Fermi surfaces of a complicated band. The ratio of $T_c/T_F \sim 0.01$ is comparable to those obtained in high-T_c cuprates and organic $(BEDT\text{-}TTF)_2$-X compounds, as demonstrated in Fig. 3 of Ref. 40. The relatively large value of T_c/T_F is in contrast to ordinary BCS superconductors with $T_c/T_F < 10^{-3}$. This feature has been discussed in detail elsewhere.[40]

VIII. DISCUSSIONS AND CONCLUSIONS

We have performed ZF μSR to investigate the SDW ordering in organic $(TMTSF)_2$-X compounds, with $X = PF_6$, NO_3, and ClO_4. The present results are generally consistent with the previous proton-NMR studies of the PF_6 and ClO_4 salts.[10,27] However, the μSR measurements directly reflect the intrinsic properties of the SDW ground state, avoiding the complexity due to the spin-flop state associated with the external field employed in NMR measurements. With the unique capability of μSR for zero-field studies, we have measured the field distribution and the SDW amplitude with statistical accuracy significantly better than previous studies. The present work has provided the first direct observation of the SDW state in the NO_3 salt, as well as the first data which allow quantitative comparison of the SDW amplitude in these three TMTSF compounds. We found evidence of a common SDW amplitude (M or μ) in PF_6, NO_3, and ClO_4 salts, which have different ordering temperatures T_{SDW}, ranging between 12 K and 4 K.

Our measurements in the PF_6 salt reveal that both the single-particle and collective-mode spin-wave excitations are important in the reduction of the sublattice magnetization M at finite T. At low temperatures, a large energy gap $\Delta_{\text{SDW}} \approx 20$ K strongly suppresses the creation of electron-hole pairs near the Fermi surface, whereas the spin-wave excitations need considerably less energy of ≈ 0.1 K. As a result, the collective-mode process becomes dominant at low temperatures. From the temperature dependence of the SDW amplitude $M(T)$ below 8 K, we obtained an average stiffness constant $\overline{D} \approx 200$ K.

Here, we see if this value of $\overline{D}$ can be explained in the framework of the Heisenberg model for localized spins. Assuming only the nearest-neighbor (NN) interaction, the spin-wave stiffness constants are $D = \alpha J_{\parallel}$ and $D' = \alpha\sqrt{J_{\parallel} J_{\perp}}$ for a spin-$\frac{1}{2}$ system, where $J_{\parallel}$ is the on-chain and $J_{\perp}$ is the interchain exchange interaction. Substituting $\alpha \approx 0.1$ and $J_{\parallel} \approx 1200$K, we expect the average stiffness $\overline{D}_{\text{NN}} \approx 120(J_{\perp}/J_{\parallel})^{1/4}$. The anisotropy ratio $J_{\perp}/J_{\parallel}$ of the exchange interaction has not been obtained yet. If we assume that this ratio is about 1/10 to 1/100 (these numbers, as we shall see, roughly correspond to weak-coupling and strong-coupling limits of the Hubbard model with $t'/t = 1/10$), then $\overline{D}_{\text{NN}} \approx 70$–$40$ K. The stiffness $\overline{D}_{\text{NN}}$, obtained from the NN Heisenberg model, is about 3–5 times smaller than the observed stiffness $\overline{D} \approx 200$ K. Note that $\overline{D}_{\text{NN}}$ is not very sensitive to the exchange anisotropy ratio. This consideration indi-

cates that the magnetism of the PF_6 compound cannot be described in the localized-moment picture.

Generally, the magnon excitations in a low-dimensional Heisenberg system (with only the NN interactions) will be enhanced due to strong thermal dynamical fluctuations. Such behavior has been observed in cuprate antiferromagnets[31] La_2CuO_4 and $Sr_2CuO_2Cl_2$, both of which have highly 2D magnetic structures. These systems exhibit a much sharper variation in the sublattice magnetization at low temperatures than that seen in 3D systems. Furthermore, $Sr_2CuO_2Cl_2$, having a more pronounced 2D character than La_2CuO_4, displays a sharper change of M. In the case of the TMTSF system, which lies somewhat between 1D and 2D systems, we expect an even faster change of M in the NN Heisenberg model. To demonstrate this, we calculated the variation of $M(T)$ expected in this model for $J_{\|} = 1200$ K, $J_{\perp} = 120$ K, and a small anisotropy energy of $\Delta = 0.2$ K, and show the results in Fig. 5 using the thin solid line. Obviously, the NN Heisenberg model is incompatible with the observed data.

The enhancement of the spin-wave stiffness constant is reminiscent of experimental results of spin-wave dispersion in itinerant ferromagnets.[41,42] For localized-moment systems, such as EuO or Pd_2MnSn, the observed stiffness constant D agrees well with a calculation in the Heisenberg model using T_c as an indicator of the exchange coupling J. For more itinerant systems, such as MnSi or Ni, the observed value of D is significantly higher than the calculated value in the above-mentioned procedure. In addition to the large energy scale for spin waves, another characteristic feature of itinerant ferromagnets is the small magnitude of the ordered moments. These two features are both seen in the TMTSF system, indicating the importance of considering the present results in terms of a crossover from a localized-moment picture to itinerant-electron magnetism. In fact, the paramagnetic states of these TMTSF compounds are essentially metallic.

To understand some general aspects of this crossover, we refer to the Hubbard model, with on-site Coulomb interaction U and on-chain transfer integral t as variable parameters. (The 1D system has been discussed by many authors.[43] In the case of a 2D half-filled band, we refer to the discussions of Schrieffer *et al.*[44]) The localized-moment picture corresponds to the limit $U/t \gg 1$, while the itinerant-electron model corresponds to $U/t \ll 1$. Figure 13(a) schematically illustrates the behavior of the effective on-chain exchange interaction J_{eff}, μ, and the ordering temperature T_{SDW} as a function of U/t. In the localized limit, one expects a full spin moment μ and $J_{\text{eff}} \sim t^2/U$. J_{eff} decreases with increasing U/t, resulting in reduction of the ordering temperature T_{SDW}. The energy scale of J_{eff} can be estimated from the perpendicular susceptibility $\chi_{\perp} \propto 1/J_{\text{eff}}$, which is independent of the size of the moment μ.

For the limit of $U/t \ll 1$, $\chi_{\perp}$ becomes the Pauli susceptibility, and thus $\chi_{\perp} \propto N(\epsilon_F) \propto 1/\epsilon_F$, where ϵ_F is the Fermi energy and $N(\epsilon)$ is the density of states. This argument leads to $J_{\text{eff}} \sim \epsilon_F \sim t$, as shown by the dashed line in Fig. 13(a). The itinerant limit naturally results in diminishing moment μ and reduced T_{SDW}. The spin-wave stiffness constant D of itinerant-electron magnets has been studied, for example, in 1D system[45] where $D = 2t\sin(\pi\rho/2)$ (where ρ refers to number of electrons per molecule) and in the half-filled 2D band $D \sim t$. Note that J_{eff} and D essentially represent the same energy scale of the system.

Special consideration is required for estimating the ordering temperature T_{SDW}. The plot in Fig. 13(a) does not involve any effect of dimensionality (or fluctuations) and relates only to the maximum value of T_{SDW} for perfect nesting. In low-dimensional systems, T_{SDW} is determined not only by the energy scales U and t, but also by the anisotropy. Here, the interchain coupling t' plays an essential role. When t' is very small, the system becomes very close to a purely 1D system, where T_{SDW} decreases with decreasing t'. We call this region the "fluctuation" region, because the phase transition is suppressed by fluctuations in low-dimensional systems. On the other hand, a further increase of t' breaks the ideal nesting situation of the Fermi surface, destroying the very reason for the Peierls transition, and thus results in a reduction of T_{SDW}, as illustrated in Fig. 13(b).

We note that in the PF_6 system, the transfer integrals have three energy scales due to the strongly anisotropic band structure: $t_1' = 0.025$ and $t_2' = 0.001$ eV (according to Ref. 1), in addition to the strongest on-chain coupling t. In the mean-field model for the itinerant electrons, t_1' plays the dominant role in determining t' in Fig. 13(b),

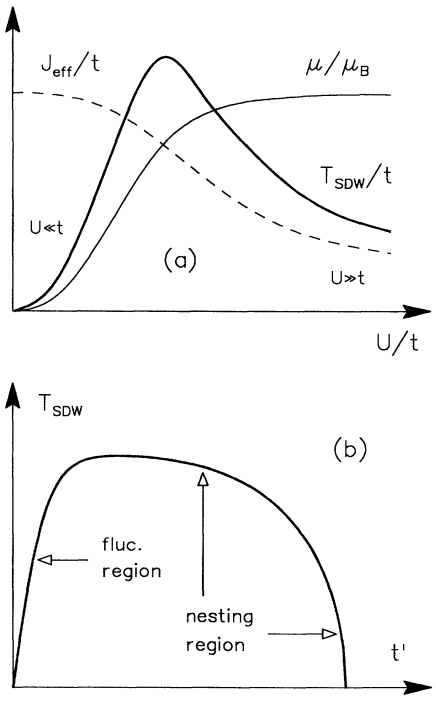

FIG. 13. Schematic results of Hubbard model. (a) Effective exchange interaction J_{eff}, moment μ, and ordering temperature T_{SDW} under weak and strong U limits. (b) Effects of transverse coupling t' on SDW transition temperature.

as can be seen in the 2D nesting model,[15] leading to the SDW transition. In the NN Heisenberg model for localized moments, where a finite t_2' or a small anisotropy energy is required to stabilize long-range order, t_2' could also play an essential role.

Let us now consider where the TMTSF systems fall in the general picture of Fig. 13. In the PF_6 salt, the ordered moment μ is reduced to about 0.1 μ_B/molecule. The observed stiffness $\overline{D}$ is several times larger than the value expected in the localized-moment model. These results clearly indicate that the system lies far from the large U/t region.

To consider in terms of an itinerant picture, one needs to estimate the transfer energies t and t'. Optical results[46] indicate $t \approx 0.25$ eV, while t' is model dependent. A simple analysis of optical data using a cylindrical Fermi surface[46] leads to $t'/t \sim 1/100$. This estimate is, however, inconsistent with the anisotropy ratio of conductivity, $\sigma'/\sigma \sim (t'/t)^2$. The conductivity measurements[28] $\sigma'/\sigma \approx 1/200$ suggest $t'/t \sim 0.1$. This value also agrees with the optical results of $t' = 0.025$ eV, assuming a band energy of $\epsilon_k = 2t\cos(ka)_{\|} + 2t'\cos(ka)_{\perp}$ with an open Fermi surface. For a quarter-filled band, $\rho = 1/2$, the stiffness constant $D = \sqrt{2}t$. Assuming $D'/D \sim t'/t$, we obtain $\overline{D} \approx \sqrt{2tt'}$. Then the itinerant model predicts $\overline{D} \approx 1300$ K for $t' = 0.025$ eV and 400 K for $t' = 0.0025$ eV. These values range somewhat higher than the observed value $\overline{D} \approx 200$ K.

The observed value $\overline{D} \approx 200$ K is derived using Eq. (5) to account for the dispersion and density of states. This equation, however, is obtained for the localized-moment model. Unfortunately, we do not have a reliable formula to replace Eq. (5) for the itinerant model. This could be a possible source of difference between observed $\overline{D}$ and the above itinerant-model calculation. Another possible source of difference is the uncertainty in the estimated value of t'. In any case, it seems that the $(TMTSF)_2PF_6$ system lies somewhat between the localized and itinerant limit.

We found that the SDW amplitude μ (or M) is nearly independent of system for the three TMTSF compounds. As shown in Fig. 13(a), μ is essentially determined by U and t, but not by t'. Therefore, the present results indicate that the three TMTSF systems have approximately same t and U. This observation is consistent with optical measurements (p. 77 of Ref. 2), which found nearly same plasma frequency ω_p along the chain direction (also indicating approximately the same t) in the PF_6 and ClO_4 salts.

The result that T_{SDW} decreases with increasing dimensionality, i.e., with increasing t', has been established by conductivity[28–30] and NMR measurements,[27] and also observed by the present μSR studies in the three systems. This clearly indicates that these TMTSF systems lie in the "nesting region" in Fig. 13(b). The results of $2\Delta \approx 3.5T_{SDW}$ found in transport measurements[22] have been also taken as evidence for relatively weak fluctuations in the TMTSF system. On the other hand, the observed sharp onset of M below T_{SDW} and the possible first-order transition suggest that the suppression of T_{SDW} due to spin fluctuations still plays an important role in determining T_{SDW}.

Our penetration-depth results for the relaxed state of the ClO_4 salt reveal that the energy scale for superconducting carriers in this system is as low as 70 K. The carrier density is only about 3% of the number expected for one carrier per formula unit. In the 2D organic superconductor $(BEDT\text{-}TTF)_2Cu(NCS)_2$, recent muon-spin-relaxation measurements of the penetration depth[47] found that the superconducting carrier density is only about 20% of one carrier per formula unit. These results indicate that the spectral weight contributing to the supercurrent below T_c is only part of the total spectral weight. We point out that this seems to be a common feature in "exotic" superconductors having highly correlated electronic structures (see Uemura *et al.*[40] for more details).

The present study demonstrates that the μSR technique is very useful in observing the magnetic behavior of organic systems. In order to study a wider range of compounds, possibly lying in different regions of Figs. 13(a) and 13(b), we are currently extending the measurements to other organic magnetic systems, including a 2D system $(BEDT\text{-}TTF)_2Cu[N(CN)_2]Cl$.[48]

ACKNOWLEDGMENTS

The authors thank G. Saito for stimulating discussions. Work at Columbia is supported by the NSF (DMR-89-13784) and the David and Lucile Packard Foundation. Work at TRIUMF is supported by NSERC and NRC. Work at Princeton is supported by the NSF (DMR-88-22532). Work at UCLA is supported by the NSF (DMR-90-06736).

* Present address: Physics Department, Brookhaven National Laboratory, Upton, New York 11973.

[1] D. Jérome and H. J. Schulz, Adv. Phys. **31**, 299 (1982).
[2] T. Ishiguro and K. Yamaji, *Organic Superconductors* (Springer-Verlag, Berlin, 1990).
[3] D. Jérome *et al.*, J. Phys. (Paris) Lett. **41**, L95 (1980); K. Andres *et al.*, Phys. Rev. Lett. **45**, 1449 (1980).
[4] H. Schwenk *et al.*, Phys. Rev. B **29**, 500 (1984).
[5] T. Takahashi *et al.*, J. Phys. (Paris) Lett. **43**, L565 (1982); S. Tomić *et al.*, *ibid.* **43**, L839 (1982).
[6] K. Bechgaard *et al.*, Phys. Rev. Lett. **46**, 852 (1981).
[7] A. Mazaud, third-cycle thesis, Université Paris-Sud, Orsay, 1981; W. Kang *et al.*, Phys. Rev. Lett. **65**, 2812 (1990).
[8] J. C. Scott *et al.*, Phys. Rev. Lett. **45**, 2125 (1980); K. Mortensen *et al.*, *ibid.* **46**, 1234 (1981); Phys. Rev. B **25**, 3319 (1982).
[9] J. B. Torrance *et al.*, Phys. Rev. Lett. **49**, 881 (1982); W. M. Walsh, Jr. *et al.*, *ibid.* **49**, 885 (1982).
[10] T. Takahashi *et al.*, J. Phys. Soc. Jpn. **55**, 1364 (1986); Physica (Amsterdam) B **143**, 417 (1986); J. M. Delrieu *et*

al., *ibid.* **143**, 412 (1986); J. Phys. (Paris) **47**, 839 (1986).
[11] L. P. Le *et al.*, Europhys. Lett. **15**, 547 (1991).
[12] A. Schenck, *Muon Spin Rotation Spectroscopy: Principles and Applications in Solid State Physics* (Hilger, Bristol, 1986).
[13] F. N. Gygax *et al.*, Europhys. Lett. **4**, 473 (1987); E. H. Brandt, Phys. Rev. B **37**, 2349 (1988); Y. J. Uemura *et al.*, Phys. Rev. Lett. **62**, 2317 (1989).
[14] In our preliminary report (Ref. 11), we used $\Delta H_{\text{p.p.}} - \Delta H_{\text{p.p.}}(T > T_{\text{SDW}})$ to represent the SDW amplitude. However, one of the authors (Takahashi) of the original NMR experiments (Ref. 10) suggested to us that $\Delta H_{\text{p.p.}}$ itself corresponds to the order parameter. Above T_{SDW}, $\Delta H_{\text{p.p.}}$ shows the background broadening.
[15] K. Yamaji, J. Phys. Soc. Jpn. **51**, 2787 (1982).
[16] L. D. Landau and E. M. Lifshitz, *Statistical Physics* (Pergamon, London, 1959).
[17] See review articles by H. J. Schulz, in *Low-Dimensional Conductors and Superconductors*, edited by D. Jérome and L. G. Caron, Vol. 155 of *NATO Advanced Study Institute, Series B: Physics* (Plenum, New York, 1987).
[18] P. A. Lee, T. M. Rice, and P. W. Anderson, Phys. Rev. Lett. **31**, 462 (1973).
[19] W. Kang *et al.*, Phys. Rev. B **41**, 4862 (1990).
[20] W. G. Clark *et al.* (private communication).
[21] A. Arrott *et al.*, Phys. Rev. Lett. **14**, 1022 (1965); S. A. Werner *et al.*, Phys. Rev. **155**, 528 (1967).
[22] P. M. Chaikin *et al.*, Phys. Rev. B **24**, 7155 (1981).
[23] J. C. Scott, Mol. Cryst. Liq. Cryst. **79**, 49 (1982).
[24] M. E. Lines, Phys. Rev. **135**, A1336 (1964).
[25] For the mean-field approximation, $J = \mu_B^2/\chi_\perp$. Using $\chi_\perp = 1.25 \times 10^{-4}$ emu/mol obtained from Ref. 8, $J = 3000$ K. (Note that the value $J = 700$ K obtained in Ref. 23 is mistaken by numerical calculation.) For the exact solution of the 1D Heisenberg model, a factor of $(2/\pi)^2$ is taken into account, due to quantum fluctuations. Then $J = 1200$ K. (Note that this value is a factor of 2 larger than that obtained in Ref. 9, due to the different definitions of J.)
[26] K. Bechgaard *et al.*, Solid State Commun. **33**, 1119 (1980); K. Mortensen *et al.*, J. Phys. (Paris) Colloq. **44**, C3-963 (1983).
[27] T. Takahashi *et al.*, J. Phys. Soc. Jpn. **58**, 703 (1989).
[28] C. S. Jacobsen *et al.*, Solid State Commun. **38**, 423 (1981).
[29] R. L. Greene *et al.*, Phys. Rev. Lett. **45**, 1587 (1980).
[30] K. Murata *et al.*, J. Phys. Soc. Jpn. **50**, 3529 (1981).
[31] L. P. Le *et al.*, Phys. Rev. B **42**, 2182 (1990); Hyperfine Interact. **63**, 279 (1990).
[32] N. Kinoshita *et al.*, J. Phys. Soc. Jpn. **53**, 1504 (1984).
[33] L. P. Le *et al.*, Chem. Phys. Lett. **206**, 405 (1993).
[34] E. Barthel *et al.*, Europhys. Lett. **21**, 87 (1993).
[35] Strictly speaking, what we rule out here is the existence of those relatively slow dynamic effects which appear in the μSR time window. For spin-wave or other spin dynamic fluctuations related to the exchange interaction, their fluctuation rates are too fast to be observed by μSR.
[36] G. M. Luke *et al.*, Phys. Lett. A **157**, 173 (1991).
[37] K. Murata *et al.*, Jpn. J. Appl. Phys. **26**, Suppl. **26-3**, 1367 (1987).
[38] P. Garoche *et al.*, J. Phys. (Paris) Lett. **43**, L147 (1982).
[39] S. Tomić *et al.*, Phys. Rev. Lett. **62**, 462 (1989).
[40] (a) Y. J. Uemura *et al.*, Phys. Rev. Lett. **66**, 2665 (1991); (b) Synthetic Metals **56**, 2845 (1993).
[41] G. Shirane *et al.*, J. Appl. Phys. **39**, 383 (1968); H. A. Mook *et al.*, *ibid.* **40**, 1450 (1969); L. Passell *et al.*, Phys. Rev. B **14**, 4897 (1976); Y. Ishikawa *et al.*, *ibid.* **16**, 4956 (1977); **25**, 254 (1982); G. Shirane *et al.*, *ibid.* **31**, 1227 (1985).
[42] Neutron-scattering results on five different ferromagnets ranged from the localized-moment to itinerant-electron systems were discussed by Y. J. Uemura, *Proceedings of the 1984 Workshop on High-Energy Excitations in Condensed Matter* (Los Alamos Natl. Lab. LA-10227, Los Alamos, 1984), p. 264.
[43] H. Shiba, Phys. Rev. B **6**, 930 (1972); D. J. Klein and W. A. Seitz, *ibid.* **10**, 3217 (1974).
[44] J. R. Schrieffer *et al.*, Phys. Rev. B **39**, 11 663 (1989).
[45] M. Takahashi, Prog. Theor. Phys. (Tokyo) **43**, 1619 (1970).
[46] C. S. Jacobsen *et al.*, Phys. Rev. Lett. **46**, 1142 (1981).
[47] Y. J. Uemura *et al.*, in *Organic Superconductivity*, edited by V. Z. Kresin and W. A. Little (Plenum, New York, 1990); L. P. Le *et al.*, Phys. Rev. Lett. **68**, 1923 (1992).
[48] U. Welp *et al.*, Phys. Rev. Lett. **69**, 840 (1992).